GPS Solut
DOI 10.1007/s10291-013-0329-5

ORIGINAL ARTICLE

Robustness of GNSS integer ambiguity resolution in the presence of atmospheric biases

Bofeng Li · Sandra Verhagen · Peter J. G. Teunissen

Received: 6 April 2013 / Accepted: 28 May 2013

Abstract Both the underlying model strength and biases are two crucial factors for successful integer GNSS ambiguity resolution (AR) in real applications. In some cases, the biases can be adequately parameterized and an unbiased model can be formulated. However, such parameterization will, as trade-off, reduce the model strength as compared to the model in which the biases are ignored. The AR performance with the biased model may therefore be better than with the unbiased model, if the biases are sufficiently small. This would allow for faster AR using the biased model, after which the unbiased model can be used to estimate the remaining unknown parameters. We assess the bias-affected AR performance in the presence of tropospheric and ionospheric biases and compare it with the unbiased case. As a result, the maximum allowable biases are identified for different situations where CORS, static and kinematic baseline models are considered with different model settings. Depending on the size of the maximum allowable bias, a user may decide to use the biased model for AR or to use the unbiased model both for AR and estimating the other unknown parameters.

B. Li (✉) · P. J. G. Teunissen
College of Surveying and Geo-Informatics, Tongji University, Shanghai, People's Republic of China
e-mail: bofeng_li@163.com; bofeng_li@tongji.edu.cn

P. J. G. Teunissen
e-mail: p.teunissen@curtin.edu.au

B. Li · P. J. G. Teunissen
GNSS Research Centre, Curtin University, Perth, Australia

S. Verhagen · P. J. G. Teunissen
Delft University of Technology, Delft, The Netherlands
e-mail: a.a.verhagen@tudelft.nl

Keywords Ambiguity resolution · Bias-affected success rate · Tropospheric biases · Ionospheric biases · Ps-LAMBDA

Introduction

High-precision GNSS (Global Navigation Satellite Systems) applications rely on the successful carrier-phase integer ambiguity resolution (AR). Solving the GNSS model is usually done based on a three-step procedure (Teunissen 1995). First, the so-called float solution, e.g., based on standard least squares, is obtained by ignoring the integer constraints on the ambiguities. Second, an integer mapping is applied to the float ambiguity solution to compute its integer counterpart. Finally, the remaining unknown parameters are adjusted using the integer ambiguity solution, since the carrier-phase observations are now unambiguous and act as very precise pseudo range measurements.

Both the underlying model strength and inadequately modelled biases are two factors affecting the probability of correct integer estimation, called success rate. This probability is defined as the integral of the float ambiguity probability density function (PDF) over the pull-in region centered at the correct integer. A pull-in region is the region centered at an integer and containing all possible real-valued solutions that are mapped to this specific integer (Teunissen 1999). With a strong model, the float solution is precise and the PDF will be peaked, which will thus result in a very high success rate if the model is unbiased. A biased solution implies that the PDF is shifted and not centered at the correct integer anymore. However, a small bias may still be acceptable in case of a strong model as it will hardly change the success rate (Teunissen 2001).

Published online: 16 July 2013

Obviously, the impact of model strength and biases must be traded off with each other in order to decide whether to use the *unbiased* or *biased* model for AR. The reason is that with the unbiased model, the biases are explicitly modelled and thus an unbiased solution is obtained. However, the precision will be reduced as compared to the solution obtained with the biased model, since in that case the biases are ignored and hence less unknown parameters are involved. This comes at the price of a biased solution. If the AR performance with the biased model is better than with the unbiased model, i.e., the impact of the biases on the success rate is less than the impact of the difference in precision, this would allow for faster AR using the biased model. Once the integer ambiguities are solved based on the biased model, the remaining unknown parameters can be estimated using the unbiased model. In other words, steps 1 and 2 of the aforementioned AR procedure can be based on the biased model, whereas for the third step, the unbiased model is used.

A classic application of bias-affected AR is to solve certain linear ambiguity combinations, which are selected such that the impact of the atmospheric biases will not affect the success rate. Examples can be found in Hatch (1982); Allison (1991); Goad (1992) with dual-frequency widelane AR and in Vollath et al. (1998); Hatch et al. (2000); Teunissen et al. (2002); Feng (2008); Li et al. (2010a) with triple-frequency cascading AR.

Teunissen et al. (2000) studied the AR robustness to ionospheric biases with the dual- and triple-frequency geometry-free model of one double-difference satellite pair by comparing the ionosphere-biased and ionosphere-float (unbiased) success rates, see also Joosten and Teunissen (2001). The result showed that an ionospheric bias of a few centimeters can decrease the single-epoch ambiguity success rate to a much lower value. Still, the ionosphere-biased model can be used, provided that additional epochs are used to push the success rate up to an acceptable level. The number of additional epochs needed is much lower than would be needed with the unbiased model. The multipath robustness of AR was analyzed in Joosten and Irsigler (2003); Kubo and Yasuda (2003); Verhagen et al. (2007) but only a qualitative assessment was made due to the complex nature of the multipath bias. Henkel and Günther (2010) proposed a method to conservatively take into account biases based on a partial AR strategy specifically for precise point positioning applications.

Bias-affected AR has been commonly used in real applications, and the AR robustness to some biases has been qualitatively analyzed in previous works. An important open question is still how to decide whether or not to use the biased or unbiased model for AR. The problem is that the bias-affected success rate can only be evaluated once the biases are known, which is obviously not the case in real applications. Therefore, a quantitative analysis is made in this research, where the biases due to troposphere and ionosphere delays will be considered. The idea is to compare the AR performance in terms of success rates obtained with the unbiased and biased models, and the resulting times to fix the ambiguities in both cases. This will be done for different cases by distinguishing the CORS, static and kinematic baseline models and different choices for the stochastic model. The size of the biases will be varied, and as such, it will be possible to determine the maximum allowable bias, such that the AR performance with the biased model is still better than with the unbiased model.

In section "Integer ambiguity estimation with unbiased and biased model," the integer AR theory in the absence and presence of biases is presented. The success rate evaluation in both cases will be reviewed in section "Success rate of ambiguity resolution." The models and simulation results for the troposphere-biased and ionosphere-biased cases are presented in sections "Ambiguity resolution with tropospheric biases" and "Ambiguity resolution with ionospheric biases," respectively. The research findings are summarized in section "Concluding remarks."

Integer ambiguity estimation with unbiased and biased model

In this section, the mathematical models of unbiased and biased ambiguity estimation are presented, followed by their corresponding three-step estimation procedures.

Integer ambiguity resolution with unbiased model

The mixed integer GNSS linear(ized) model is defined as

$$\mathrm{E}(\boldsymbol{y}) = \boldsymbol{A}\boldsymbol{a} + \boldsymbol{B}\boldsymbol{b} + \boldsymbol{C}\boldsymbol{\nabla},\ \mathrm{D}(\boldsymbol{y}) = \boldsymbol{Q}_{\boldsymbol{yy}} \tag{1}$$

where E and D denote the expectation and dispersion operators. $\boldsymbol{a} \in \mathbb{Z}^n$, $\boldsymbol{b} \in \mathbb{R}^p$ and $\boldsymbol{\nabla} \in \mathbb{R}^q$ are the integer ambiguity, baseline and other nuisance parameter vectors, respectively. Their design matrices are $\boldsymbol{A} \in \mathbb{R}^{m\times n}$, $\boldsymbol{B} \in \mathbb{R}^{m\times p}$ and $\boldsymbol{C} \in \mathbb{R}^{m\times q}$ with $[\boldsymbol{A}\ \boldsymbol{B}\ \boldsymbol{C}]$ of full column rank. The observation vector $\boldsymbol{y} \in \mathbb{R}^m$ contains the double-difference (DD) code and phase observations and is assumed to be contaminated by normally distributed random noises with zero means and variance–covariance (VC-)matrix $\boldsymbol{Q}_{\boldsymbol{yy}}$. It is emphasized that the nuisance parameter $\boldsymbol{\nabla}$ is set up to compensate the non-ignorable systematic biases for which in this paper the tropospheric and ionospheric biases will be considered. In general, a three-step procedure is employed to solve model (1) based on the least squares criterion.

Step 1: Float solution
The integer property of the ambiguities $\boldsymbol{a} \in \mathbb{Z}^n$ is disregarded, and the so-called float solution is computed,

$$\begin{bmatrix} \hat{\boldsymbol{a}} \\ \hat{\boldsymbol{b}} \end{bmatrix} \sim \mathrm{N}\left(\begin{bmatrix} \boldsymbol{a} \\ \boldsymbol{b} \end{bmatrix}, \begin{bmatrix} \boldsymbol{Q}_{\hat{a}\hat{a}} & \boldsymbol{Q}_{\hat{a}\hat{b}} \\ \boldsymbol{Q}_{\hat{b}\hat{a}} & \boldsymbol{Q}_{\hat{b}\hat{b}} \end{bmatrix} \right) \tag{2}$$

where

$$\begin{bmatrix} \boldsymbol{Q}_{\hat{a}\hat{a}} & \boldsymbol{Q}_{\hat{a}\hat{b}} \\ \boldsymbol{Q}_{\hat{b}\hat{a}} & \boldsymbol{Q}_{\hat{b}\hat{b}} \end{bmatrix} = \begin{bmatrix} \boldsymbol{A}^T\bar{\boldsymbol{Q}}_{yy}^{-1}\boldsymbol{A} & \boldsymbol{A}^T\bar{\boldsymbol{Q}}_{yy}^{-1}\boldsymbol{B} \\ \boldsymbol{B}^T\bar{\boldsymbol{Q}}_{yy}^{-1}\boldsymbol{A} & \boldsymbol{B}^T\bar{\boldsymbol{Q}}_{yy}^{-1}\boldsymbol{B} \end{bmatrix}^{-1} \tag{3a}$$

$$\bar{\boldsymbol{Q}}_{yy}^{-1} = \boldsymbol{Q}_{yy}^{-1} - \boldsymbol{Q}_{yy}^{-1}\boldsymbol{C}(\boldsymbol{C}^T\boldsymbol{Q}_{yy}^{-1}\boldsymbol{C})^{-1}\boldsymbol{C}^T\boldsymbol{Q}_{yy}^{-1} \tag{3b}$$

Only the float solution of the ambiguity and baseline parameters is presented, since the goal is to investigate the impact of unmodelled biases $\boldsymbol{\nabla}$.

Step 2: Integer estimation
The float ambiguity estimate $\hat{\boldsymbol{a}}$ is used to compute its integer counterpart, denoted as

$$\check{\boldsymbol{a}} = I(\hat{\boldsymbol{a}}) \tag{4}$$

with $I : \mathbb{R}^n \mapsto \mathbb{Z}^n$ the integer mapping from the reals to the integers in n-dimensional space. There are different choices of mapping function I possible, which correspond to different integer estimation methods. Integer rounding, integer bootstrapping and integer least squares (ILS) are examples of such integer estimators. Of all choices, ILS is optimal as it can achieve the largest success rate (Teunissen 1999). ILS is efficiently mechanized in the LAMBDA method (Teunissen 1993; de Jonge and Tiberius 1996; Li and Teunissen 2011). Recently, a new version of the LAMBDA software (version 3.0) was released with a more efficient search strategy and more integer estimation methods (Verhagen and Li 2012).

Step 3: Fixed solution
The float solution of the baseline parameters is updated using the fixed integer parameters,

$$\check{\boldsymbol{b}} = \hat{\boldsymbol{b}} - \boldsymbol{Q}_{\hat{b}\hat{a}}\boldsymbol{Q}_{\hat{a}\hat{a}}^{-1}(\hat{\boldsymbol{a}} - \check{\boldsymbol{a}}) \tag{5a}$$

$$\boldsymbol{Q}_{\check{b}\check{b}} = \boldsymbol{Q}_{\hat{b}\hat{b}} - \boldsymbol{Q}_{\hat{b}\hat{a}}\boldsymbol{Q}_{\hat{a}\hat{a}}^{-1}\boldsymbol{Q}_{\hat{a}\hat{b}} \tag{5b}$$

It is pointed out that the VC matrix $\boldsymbol{Q}_{\check{b}\check{b}}$ is derived based on the error propagation law with assumption that the integer solution $\check{\boldsymbol{a}}$ is deterministic. This holds true only when the success rate is sufficiently close to 1. In that case, $\boldsymbol{Q}_{\check{b}\check{b}} \ll \boldsymbol{Q}_{\hat{b}\hat{b}}$ since after successful ambiguity fixing, the carrier-phase measurements start to act as very precise pseudorange measurements. However, if the success rate is not sufficiently high, the fixed solution $\check{\boldsymbol{b}}$ is not necessarily more precise than the float solution $\hat{\boldsymbol{b}}$ (de Jonge et al. 2000; Verhagen et al. 2013).

Integer ambiguity resolution with biased model

If $\boldsymbol{\nabla} = \boldsymbol{0}$ holds true in (1), unbiased parameter estimation is obtained using the reduced model

$$\mathrm{E}(\boldsymbol{y}) = \boldsymbol{A}\boldsymbol{a} + \boldsymbol{B}\boldsymbol{b}, \quad \mathrm{D}(\boldsymbol{y}) = \boldsymbol{Q}_{yy} \tag{6}$$

However, if $\boldsymbol{\nabla} \neq \boldsymbol{0}$, i.e., if the atmospheric biases are not so small to be completely ignorable, biased parameter estimates will be obtained with (6).

In principle, reducing the parameters in an adjustment system can improve the model strength but as trade-off introduces biases in the parameter estimates if the systematic effects specified by these parameters cannot be completely ignored. The three-step procedure for solving model (6) in the presence of atmospheric biases ($\boldsymbol{\nabla} \neq \boldsymbol{0}$) will thus lead to a biased solution, as described next.

Step 1: Float solution
The float solution is again obtained by disregarding the integer constraints on the ambiguities,

$$\begin{bmatrix} \hat{\boldsymbol{a}}^{\mathrm{b}} \\ \hat{\boldsymbol{b}}^{\mathrm{b}} \end{bmatrix} \sim \mathrm{N}\left(\begin{bmatrix} \boldsymbol{a} + \Delta\boldsymbol{a} \\ \boldsymbol{b} + \Delta\boldsymbol{b} \end{bmatrix}, \begin{bmatrix} \boldsymbol{Q}^{\mathrm{b}}_{\hat{a}\hat{a}} & \boldsymbol{Q}^{\mathrm{b}}_{\hat{a}\hat{b}} \\ \boldsymbol{Q}^{\mathrm{b}}_{\hat{b}\hat{a}} & \boldsymbol{Q}^{\mathrm{b}}_{\hat{b}\hat{b}} \end{bmatrix} \right) \tag{7}$$

with the VC matrix

$$\begin{bmatrix} \boldsymbol{Q}^{\mathrm{b}}_{\hat{a}\hat{a}} & \boldsymbol{Q}^{\mathrm{b}}_{\hat{a}\hat{b}} \\ \boldsymbol{Q}^{\mathrm{b}}_{\hat{b}\hat{a}} & \boldsymbol{Q}^{\mathrm{b}}_{\hat{b}\hat{b}} \end{bmatrix} = \begin{bmatrix} \boldsymbol{A}^T\boldsymbol{Q}_{yy}^{-1}\boldsymbol{A} & \boldsymbol{A}^T\boldsymbol{Q}_{yy}^{-1}\boldsymbol{B} \\ \boldsymbol{B}^T\boldsymbol{Q}_{yy}^{-1}\boldsymbol{A} & \boldsymbol{B}^T\boldsymbol{Q}_{yy}^{-1}\boldsymbol{B} \end{bmatrix}^{-1} \tag{8}$$

and the bias vector

$$\begin{bmatrix} \Delta\boldsymbol{a} \\ \Delta\boldsymbol{b} \end{bmatrix} = \begin{bmatrix} \boldsymbol{Q}^{\mathrm{b}}_{\hat{a}\hat{a}} & \boldsymbol{Q}^{\mathrm{b}}_{\hat{a}\hat{b}} \\ \boldsymbol{Q}^{\mathrm{b}}_{\hat{b}\hat{a}} & \boldsymbol{Q}^{\mathrm{b}}_{\hat{b}\hat{b}} \end{bmatrix} \begin{bmatrix} \boldsymbol{A}^T\boldsymbol{Q}_{yy}^{-1}\boldsymbol{C} \\ \boldsymbol{B}^T\boldsymbol{Q}_{yy}^{-1}\boldsymbol{C} \end{bmatrix} \boldsymbol{\nabla} \tag{9}$$

where the superscripts "b" are used to denote the biased terms. It can be easily shown that the VC matrix (8) is smaller than the unbiased one (3) and also $\boldsymbol{Q}^{\mathrm{b}}_{\hat{a}\hat{a}} \leq \boldsymbol{Q}_{\hat{a}\hat{a}}$ and $\boldsymbol{Q}^{\mathrm{b}}_{\hat{b}\hat{b}} \leq \boldsymbol{Q}_{\hat{b}\hat{b}}$. The reason is that the number of unknown parameters is reduced.

Step 2: Integer estimation
Similarly as with the unbiased model, the float ambiguity estimate $\hat{\boldsymbol{a}}^{\mathrm{b}}$ is used to compute its integer counterpart:

$$\check{\boldsymbol{a}}^{\mathrm{b}} = I(\hat{\boldsymbol{a}}^{\mathrm{b}}) \tag{10}$$

Step 3: Fixed solution
Once the ambiguities are fixed by applying Steps 1 and 2 described here, one should never disregard the biases for computing the precise baseline solution, since even if $\check{\boldsymbol{a}}^{\mathrm{b}}$ is correct, the bias $\Delta\boldsymbol{b}$ will propagate in the fixed baseline solution. Therefore, the unbiased float estimates from (2) must be used and (5) is adjusted to:

$$\check{\boldsymbol{b}} = \hat{\boldsymbol{b}} - \boldsymbol{Q}_{\hat{b}\hat{a}}\boldsymbol{Q}_{\hat{a}\hat{a}}^{-1}\left(\hat{\boldsymbol{a}} - \check{\boldsymbol{a}}^{\mathrm{b}}\right) \tag{11a}$$

$$\boldsymbol{Q}_{\check{b}\check{b}} = \boldsymbol{Q}_{\hat{b}\hat{b}} - \boldsymbol{Q}_{\hat{b}\hat{a}}\boldsymbol{Q}_{\hat{a}\hat{a}}^{-1}\boldsymbol{Q}_{\hat{a}\hat{b}} \tag{11b}$$

This is equivalent to solving the model

$$\mathrm{E}(\boldsymbol{y} - \boldsymbol{A}\check{\boldsymbol{a}}^{\mathrm{b}}) = \boldsymbol{B}\boldsymbol{b} + \boldsymbol{C}\nabla,\ \mathrm{D}(\boldsymbol{y}) = \boldsymbol{Q}_{yy} \tag{12}$$

Note from (5b) and (11b) that the precision $\boldsymbol{Q}_{\check{b}\check{b}}$ of the fixed baseline solution with $\check{\boldsymbol{a}}$ is the same as with $\check{\boldsymbol{a}}^{\mathrm{b}}$ if in both cases, the uncertainty of the fixed ambiguity solution can be ignored. Therefore, it will be better to use $\check{\boldsymbol{a}}^{\mathrm{b}}$ if the probability that this integer solution is correct is higher than that $\check{\boldsymbol{a}}$ is correct. In the next section, it will be explained that this can be the case due to the fact that $\boldsymbol{Q}_{\hat{a}\hat{a}}^{\mathrm{b}} \leq \boldsymbol{Q}_{\hat{a}\hat{a}}$.

Success rate of ambiguity resolution

The success rate for unbiased and biased ambiguity resolution is mathematically defined. Some simple examples are then presented to intuitively show why the biased ambiguity resolution can be better than the unbiased one.

Success rate with unbiased model

Integer ambiguity estimation essentially means that the real ambiguity vector $\hat{\boldsymbol{a}}$ is mapped to its integer counterpart $\breve{\boldsymbol{a}}$, by using a mapping function $I : \mathbb{R}^n \mapsto \mathbb{Z}^n$. Due to the discrete nature of $\mathbb{Z}^n$, the map I will not be one-to-one, but instead many-to-one. This implies that different real ambiguity vectors will be mapped to the same integer vector. One can therefore assign a subset $S_z \subset \mathbb{R}^n$ to each integer vector $\boldsymbol{z} \in \mathbb{Z}^n$ (Teunissen 1999):

$$S_z = \{\boldsymbol{x} \in \mathbb{R}^n | \boldsymbol{z} = I(\boldsymbol{x})\},\ \boldsymbol{z} \in \mathbb{Z}^n \tag{13}$$

This subset is referred to as the *pull-in region* of $\boldsymbol{z}$. It is the region in which all float ambiguity solutions are pulled to the same fixed ambiguity vector $\boldsymbol{z}$. This implies that the probability of correct ambiguity estimation, i.e., success rate P_s, is equal to the probability that $\hat{\boldsymbol{a}}$ resides in the pull-in region $S_{\boldsymbol{a}}$ with $\boldsymbol{a}$ the true but unknown ambiguity vector

$$P_s = P(\breve{\boldsymbol{a}} = \boldsymbol{a}) = P(\hat{\boldsymbol{a}} \in S_{\boldsymbol{a}}) = \int_{S_{\boldsymbol{a}}} f_{\hat{\boldsymbol{a}}}(\boldsymbol{x}|\boldsymbol{a})\ \mathrm{d}\boldsymbol{x} \tag{14}$$

The PDF of the normally distributed float ambiguity solution, $f_{\hat{\boldsymbol{a}}}(\boldsymbol{x}|\boldsymbol{a})$, reads

$$f_{\hat{\boldsymbol{a}}}(\boldsymbol{x}|\boldsymbol{a}) = |2\pi\boldsymbol{Q}_{\hat{a}\hat{a}}|^{-\frac{1}{2}}\exp\left\{-\frac{1}{2}\|\boldsymbol{x} - \boldsymbol{a}\|_{\boldsymbol{Q}_{\hat{a}\hat{a}}}^2\right\} \tag{15}$$

with $\|\cdot\|_{\boldsymbol{Q}}^2 = (\cdot)^T\boldsymbol{Q}^{-1}(\cdot)$. Due to the integer translation invariant property of pull-in regions, the success rate can also be evaluated as:

$$P_s = \int_{S_{\boldsymbol{0}}} f_{\hat{\boldsymbol{a}}}(\boldsymbol{x}|\boldsymbol{0})\ \mathrm{d}\boldsymbol{x} \tag{16}$$

It is observed that besides the PDF, the geometric interpretation of the pull-in region is needed for evaluation of the success rate. The ILS pull-in region is defined as (Teunissen 1999):

$$S_{z,\mathrm{ILS}} = \left\{\boldsymbol{x} \in \mathbb{R}^n \middle| |\omega_z(\boldsymbol{x})| \leq \frac{1}{2}\|\boldsymbol{u}\|_{\boldsymbol{Q}_{\hat{a}\hat{a}}}, \forall \boldsymbol{u} \in \mathbb{Z}^n\right\} \tag{17}$$

with

$$\omega_z(x) = \frac{\boldsymbol{u}^T\boldsymbol{Q}_{\hat{a}\hat{a}}^{-1}(\boldsymbol{x} - \boldsymbol{z})}{\|\boldsymbol{u}\|_{\boldsymbol{Q}_{\hat{a}\hat{a}}}}$$

being the orthogonal projection of $(\boldsymbol{x}–\boldsymbol{z})$ onto the direction vector $\boldsymbol{u}$.

Success rate with biased model

For the biased float solution $\hat{\boldsymbol{a}}^{\mathrm{b}} \sim \mathbf{N}(\boldsymbol{a} + \Delta\boldsymbol{a}, \boldsymbol{Q}_{\hat{a}\hat{a}}^{\mathrm{b}})$, the bias-affected success rate follows as

$$P_s^{\mathrm{b}} = P(\check{\boldsymbol{a}}^{\mathrm{b}} = \boldsymbol{a}) = \int_{S_{\boldsymbol{0}}} f_{\hat{\boldsymbol{a}}^{\mathrm{b}}}(\boldsymbol{x}|\Delta\boldsymbol{a})\ \mathrm{d}\boldsymbol{x} \tag{18}$$

where the PDF of the integer translated but still biased float solution $(\hat{\boldsymbol{a}}^{\mathrm{b}} - \boldsymbol{a})$ is

$$f_{\hat{\boldsymbol{a}}^{\mathrm{b}}}(\boldsymbol{x}|\Delta\boldsymbol{a}) = \left|2\pi\boldsymbol{Q}_{\hat{a}\hat{a}}^{\mathrm{b}}\right|^{-\frac{1}{2}}\exp\left\{-\frac{1}{2}\|\boldsymbol{x} - \Delta\boldsymbol{a}\|_{\boldsymbol{Q}_{\hat{a}\hat{a}}^{\mathrm{b}}}^2\right\} \tag{19}$$

In the extreme case that the biases $\nabla = 0$, the success rate P_s^{b} with the biased model will obviously be larger than with the unbiased model due to the improved precision. But also if the biases are sufficiently small, their negative impact on the success rate will be smaller than the positive impact of improved precision, so that still $P_s^{\mathrm{b}} > P_s$. This will often be the case with atmospheric biases, particularly for short baselines in GNSS applications.

A simple example will now be presented in order to illustrate how the bias-affected AR performance can indeed be better than in the unbiased case. The example is taken from Li et al. (2010b) where the regularization method is used for fast AR. The least squares float ambiguity solution and its associated regularized solution are $\hat{a} \sim \mathrm{N}(0, 0.25)$ and $\hat{a}^{\mathrm{b}} \sim \mathrm{N}(0.1, 0.09)$, respectively. The corresponding PDFs are depicted in Fig. 1. Although a 0.1 cycle bias is introduced in the regularized solution, the associated precision is improved from 0.5 to 0.3 cycles, so that the PDF is much more peaked, and consequently, the success rate is 88.6 %, which is much larger than 68.3 % for the unbiased case.

Figure 2 shows the success rate contours of bias-affected AR in one dimension, $\hat{a}^{\mathrm{b}} \sim \mathrm{N}(\Delta a, \sigma_{\hat{a}}^2)$, with varying

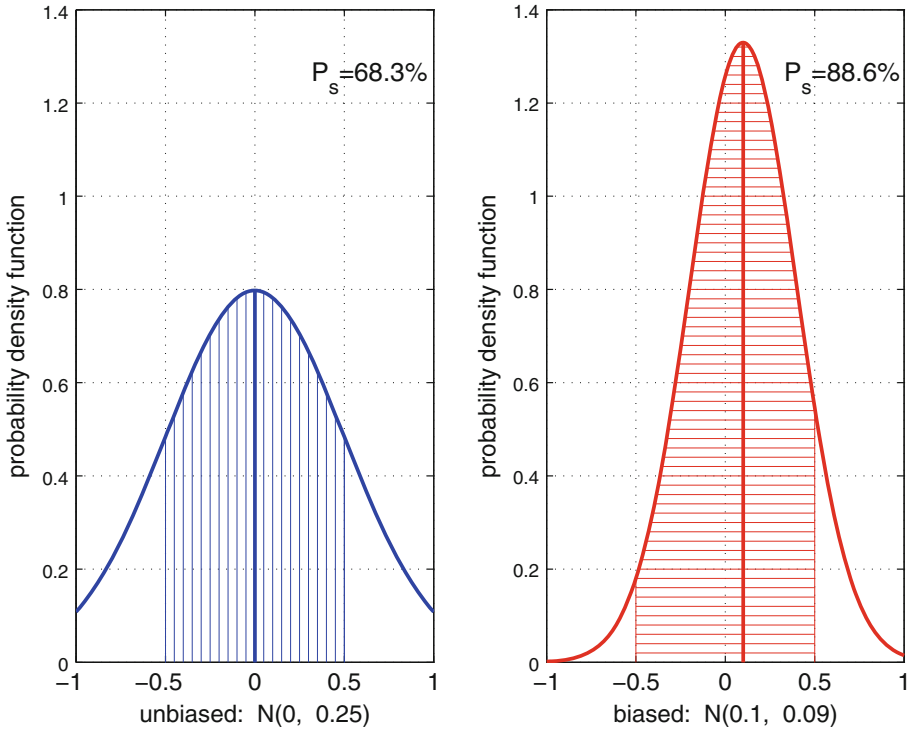

Fig. 1 One-dimensional example: PDF's of unbiased (*left*) and biased (*right*) float ambiguity solutions. *The shaded area* is equal to the success rate

biases and precisions. Clearly the decreasing trend of the success rate can be observed both for increasing bias and for increasing precision. In the unbiased case with $\Delta a = 0$, the success rates 99.9 and 99.999 % are obtained for $\sigma_{\hat{a}} = 0.152$ and $\sigma_{\hat{a}} = 0.115$ cycles, respectively. The same success rates can be achieved in the biased case with $\Delta a = 0.075$ and $\Delta a = 0.190$ if the precision is improved to 0.1 cycles.

The bias threshold of 0.5 cycles is observed from Fig. 2 for small $\sigma_{\hat{a}}$ values. If a bias is smaller than this threshold, the success rate is very high and nearly invariant; otherwise, the success rate becomes extremely small. This is because the PDF in case of high precision is very peaked such that with a small bias, most of the probability mass will still be inside the correct pull-in region, and then the success rate is hardly affected. However, with a bias larger than this threshold, nearly all the probability mass will shift to the incorrect pull-in region, and consequently, the success rate becomes suddenly very small.

Ps-LAMBDA: success rate evaluation

The geometry of the ILS pull-in region (17) is very complicated, so that exact evaluation of the success rate is generally not feasible. Hence, a variety of easy-to-use success rate approximations and bounds have been developed so far. All of them have been implemented in Ps-LAMBDA, a MATLAB software toolbox, which was released recently. For more information, one can refer to Verhagen et al. (2013) and the software can be freely downloaded from http://gnss.curtin.edu.au.

The software only needs the VC matrix of the float ambiguity solution as input. The success rates can be computed for ILS, integer bootstrapping and integer rounding. In evaluating these success rates, the users can also choose between Monte-Carlo-based approximation or lower and upper bounds. In this study, the Monte-Carlo simulation-based success rate is applied since it can give a very good approximation if the number of samples is sufficiently large, for instance, 10^6 as suggested by Verhagen et al. (2013) for most GNSS models. Moreover, the simulation-based success rate can also be used to evaluate the bias-affected success rate. The bias in the float ambiguity solution, $\Delta \boldsymbol{a}$, must then be given as input as well.

Ambiguity resolution with tropospheric biases

In this section, we study the ambiguity resolution in the absence and presence of tropospheric biases. The corresponding unbiased and troposphere-biased models are first formulated, based on which the numerical computations are executed to show the performance of troposphere-biased model compared with the unbiased model.

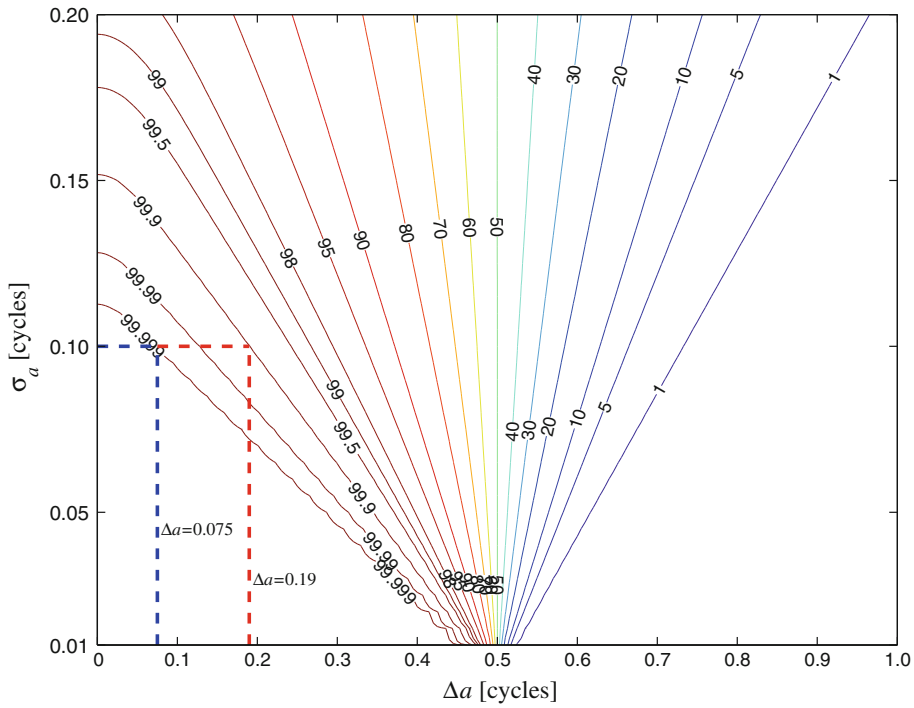

Fig. 2 Success rate contours of bias-affected AR in one dimension: $\hat{a}^{\mathrm{b}} \sim \mathrm{N}(\Delta a, \sigma_{\hat{a}}^2)$

Unbiased and troposphere-biased model

The single-epoch DD kinematic model reads

$$\mathrm{E}(\boldsymbol{y}_k) = \boldsymbol{A}\boldsymbol{a} + \boldsymbol{B}_k\boldsymbol{b}_k + \boldsymbol{G}_k\tau + \boldsymbol{E}\iota_k,\ \mathrm{D}(\boldsymbol{y}_k) = \boldsymbol{Q}_{y_k y_k} \qquad (20)$$

where the subscript k denotes the epoch number used for the epoch-specific terms; $\boldsymbol{y}_k$ is the observation vector consisting of dual-frequency DD phase and code measurements with VC matrix $\boldsymbol{Q}_{\boldsymbol{y}_k\boldsymbol{y}_k}$; $\boldsymbol{a}$, $\boldsymbol{b}_k$, τ and $\boldsymbol{\iota}_k$ are the parameters of DD ambiguities, baseline components, relative zenith troposphere delay (ZTD) and DD ionospheric biases on L1 frequency with design matrices $\boldsymbol{A}$, $\boldsymbol{B}_k$, $\boldsymbol{G}_k$ and $\boldsymbol{E}$, respectively. To enhance the model strength, the prior ionospheric corrections $\boldsymbol{\iota}_k^0$ are often applied as constraints with the statistics

$$E(\boldsymbol{\iota}_k^0) = \boldsymbol{\iota}_k, \quad D(\boldsymbol{\iota}_k^0) = \boldsymbol{Q}_{\iota\iota} = \sigma_\iota^2 \boldsymbol{D}^T\boldsymbol{D} \qquad (21)$$

where σ_ι is the standard deviation (STD) of between-receiver *single-difference* (SD) ionospheric constraint. The differential matrix $\boldsymbol{D}^T = [-\boldsymbol{e}_s \quad \boldsymbol{I}_s]$ is used to transform the $(s+1)$ SD observations to the s DD ones with the first satellite as reference. Combining (20) and (21) yields the ionosphere-weighted model.

In the following, three different baseline models will be considered, namely the CORS, the static and the kinematic baseline models. In the CORS model, the baseline parameters $\boldsymbol{b}_k$ are not estimated but held fixed. The static model differs from the kinematic model as presented above by replacing the epoch-wise baseline vector $\boldsymbol{b}_k$ with a constant vector $\boldsymbol{b}$ equal for all epochs.

In the troposphere-biased model, the relative ZTD parameter is ignored and thus eliminated from model (20). Hence, if compared to model (1), the bias $\nabla = \tau$. Note that the ionosphere parameters are added to the model as compared to models (1) and (6). For a given bias τ, the corresponding biased float solution can be computed as in (8) and (9).

Simulation setup

A GPS almanac is used to simulate four baselines in the Perth area for 24 h with a sampling interval of 5 s and cutoff elevation of 15°. An elevation-dependent weighting function is applied, and the observation variance at elevation θ is $\sigma^2(\theta) = \sigma_0^2/\sin^2\theta$ with σ_0 the STD at zenith, which takes 2 mm and 20 cm for dual-frequency undifferenced phase and code measurements, respectively. Four baseline lengths of approximately 25, 50, 100 and more than 150 km are considered, for which the ionospheric constraints are assumed to have STDs of $\sigma_\iota = 3.5$, 7.0, 14 cm and ∞, respectively. The very long baseline model is referred to as the ionosphere-float model, as it is equivalent to the model where the ionosphere delays are treated and thus estimated as completely unknown parameters without any constraints.

The success rates with the unbiased and biased models are evaluated based on Monte-Carlo simulation-based success rates with 10^6 samples. The minimum required success rate is set to $P_0 = 99.5$ %, and the time-to-first-fix (TTFF) is the number of epochs needed to meet this

requirement. The TTFF is determined for 1,440 start times during 1 day, i.e., for every minute of the day.

The tropospheric bias is varied from 0 to 3 cm. It should be stressed that this bias is not known in real applications, so that it will then be impossible to evaluate the actual bias-affected success rate. However, the simulation study presented here will compare the TTFFs with the unbiased and biased models for the different sizes of the bias. From experience, it is known what the size of tropospheric biases can be under different circumstances. If the maximum allowable bias, with which the TTFF is shorter with the unbiased model, is larger than these known values, this indicates that it is safe to work with the biased model for AR. And vice versa, if the maximum allowable bias is smaller, it is advised to use the unbiased model for AR.

Simulation results

The TTFF is determined for all models and start times. The mean, maximum and 95-percentile values over all 1,440 times are shown in Figs. 3, 4 and 5 as a function of the bias. The TTFF statistics for the unbiased model are included as well.

The TTFF will be shortest with the CORS model as compared to the static and kinematic baseline models, due to the fewer number of unknown parameters (known baseline). Furthermore, it is clear that with increasing STD σ_ι of the ionospheric constraint, the model becomes weaker and thus the TTFF will be longer.

The success rate with the biased model in case $\tau = 0$ is of course larger than with the unbiased model, since then only the gain in precision affects the success rate. The bias-affected success rate, P_s^{b}, will become smaller with increasing bias τ. This implies that more epochs of data will be required before the model is sufficiently strong to obtain $P_s^{\mathrm{b}} > 99.5\ \%$. The increasing trend for the TTFF is very strong for the longer baseline models (with larger σ_ι). For the shorter baseline, the model is already strong and it can be seen in Figs. 3, 4 and 5 that then the tropospheric bias is allowed to be rather large without a significant impact on the TTFF.

The CORS model is very strong, allowing for short TTFF, and as explained in section "Success rate with biased model," a small bias will then hardly affect the success rate. However, the precision of the CORS model will be improved very slowly with adding more epochs of data, and consequently, the success rate will not improve much either. The negative impact of larger biases on the success rate will therefore not be compensated by the improved precision from the additional epochs. This partially explains why the TTFF with the CORS model increases more rapidly for larger tropospheric biases than with the static and kinematic

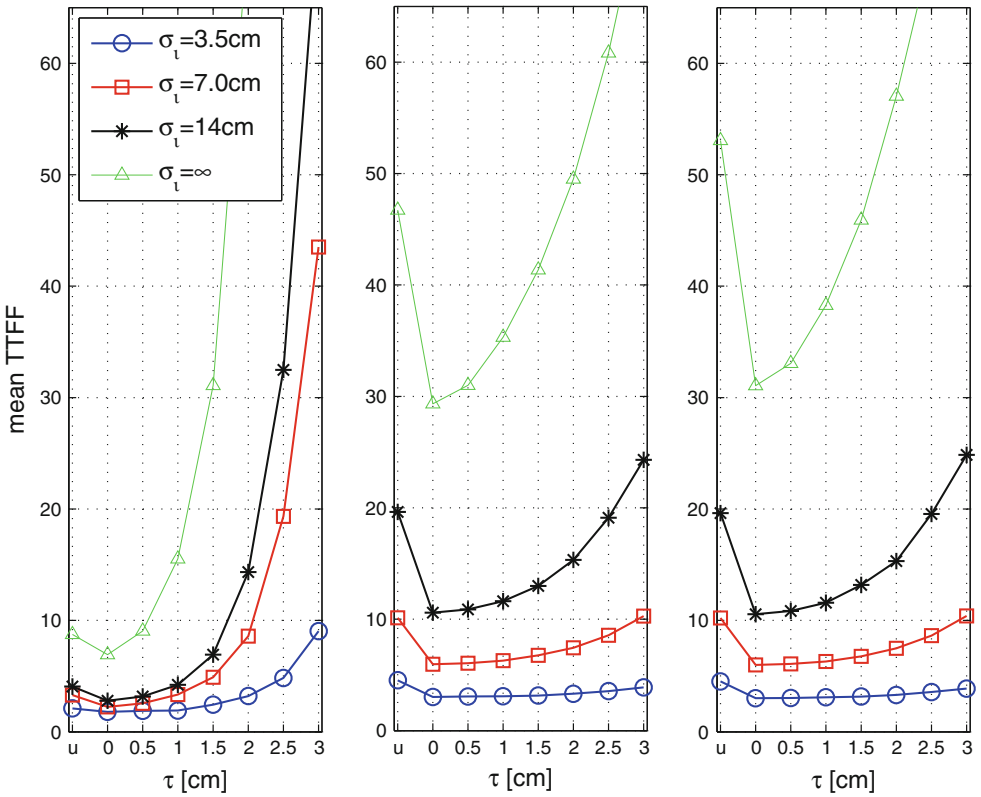

Fig. 3 The mean TTFF as function of τ. The "u" at x-label indicated the unbiased model, while the others the troposphere-biased model with different biases. The subplots from *left* to *right* denote the ionosphere-weighted CORS, static and kinematic baseline models with varying STDs of ionospheric constraints for the unbiased and troposphere-biased cases

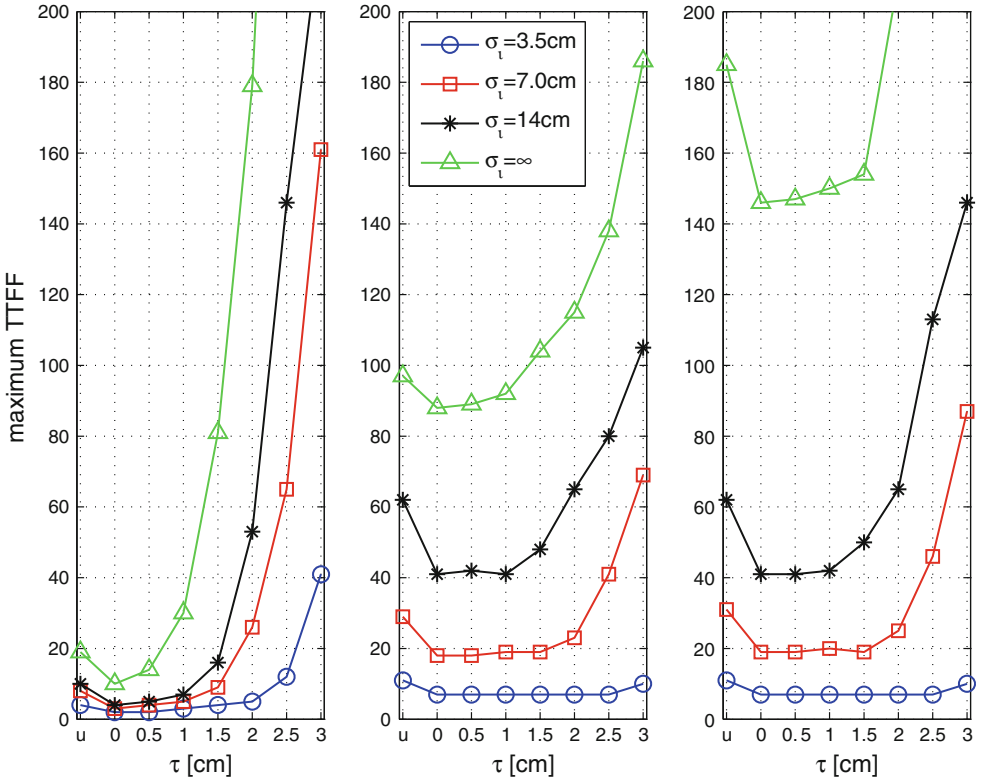

Fig. 4 The maximum TTFFs as function of τ. The "u" at x-label indicated the unbiased model, while the others the troposphere-biased model with different biases. The subplots from *left* to *right* denote the ionosphere-weighted CORS, static and kinematic baseline models with varying STDs of ionospheric constraints for the unbiased and troposphere-biased cases

baselines. In addition, the strong correlation of the relative ZTD parameter with the baseline parameters $\boldsymbol{b}$ for the static and kinematic baseline models plays a role (Li et al. 2010c). Due to this correlation, the tropospheric biases will be, to a certain extent, absorbed by the float baseline estimates, and thus, the ambiguity biases may be smaller than those with the CORS model.

The TTFF statistics in Fig. 3 are very similar for the static and kinematic baseline models, especially with small biases. In order to explain this, the extreme assumption of no satellite-receiver geometry variation over time will first be considered. This means that $\boldsymbol{B}_k = \boldsymbol{B}$, for $k = 1 \cdots r$, is thus time independent. Then, it is easy to prove that the r-epoch ambiguity VC matrix is equal to the single-epoch VC matrix scaled by $1/r$, both for the static and kinematic model (Verhagen and Joosten 2003). With the time-varying satellite-receiver geometry in the real situation, the static model should in principle be better than the kinematic model, since the geometry gain over time is fully dedicated to one unknown baseline in the static model, whereas it is neutralized due the epoch-wise unknown baselines in the kinematic model. However, in this particular case, AR usually takes a short time for the static and kinematic models with $\sigma_\iota = 3.5$, 7.0 or 14 cm. In such short time, the change in satellite-receiver geometry is too small to see the difference between both models. Nevertheless, a long TTFF is required for weak models with $\sigma_\iota = \infty$, and then the geometry variation can be remarkable, and consequently, a clear difference between both models can be observed, especially for large biases.

Choice of troposphere-biased or unbiased model

The troposphere-biased model outperforms the unbiased model for AR if the biases are smaller than the maximum allowable biases given in Table 1. These maximum biases are based on Figs. 3, 4 and 5, such that the TTFF will generally be smaller with the biased model than with the unbiased model. Recall that the TTFF is the time required to obtain a success rate (P_s^{b} or P_s) larger than 99.5 %.

To make the decision whether to adopt the bias-affected or unbiased model in real applications, the expected size of the relative ZTD bias in a real situation is examined. A 24-h dual-frequency GPS dataset from the New Zealand CORS network with 14 stations that form 91 baselines from 20 to 200 km is used (Nardo et al. 2011). After ambiguity fixing, the relative ZTDs are estimated for every 30 min for each baseline with the Bernese software (Dach et al. 2007); hence, in total, $91 \times 49 = 4{,}459$ relative ZTDs are computed. The cumulative probability distribution of the relative ZTDs is shown in Fig. 6 for different intervals of the baseline length.

The results in Fig. 6 can now be compared with the maximum allowable biases in Table 1 in order to decide whether to use the troposphere-biased or unbiased model for AR. The applicability of the following recommendations

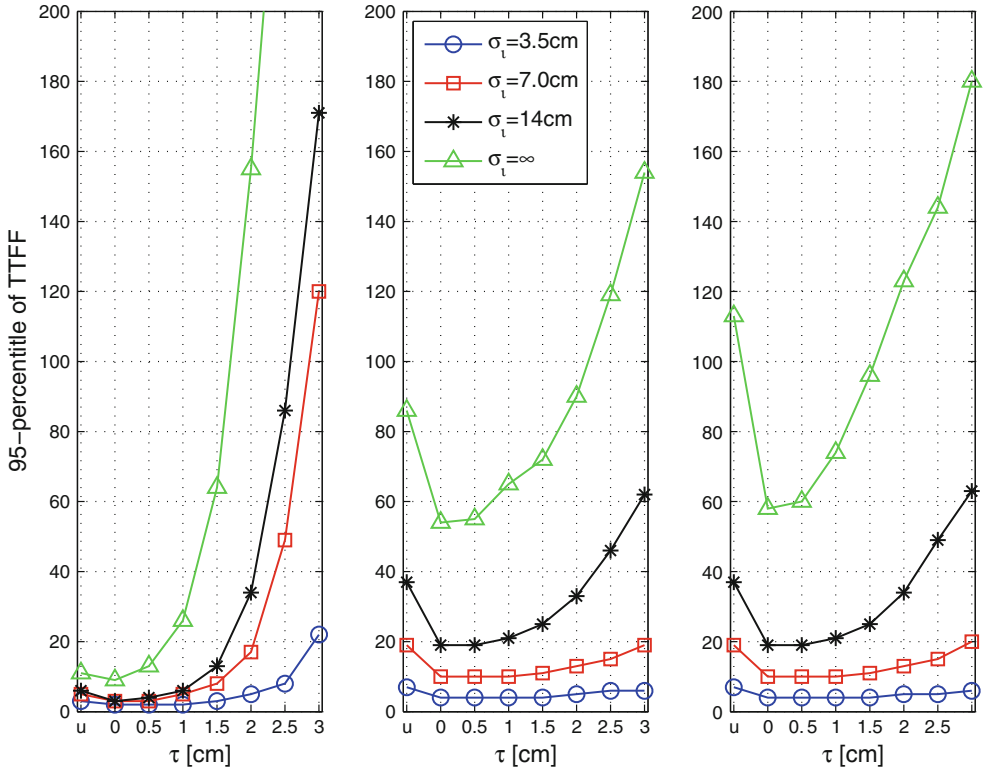

Fig. 5 The 95-percentile TTFFs as function of τ. The "u" at *x*-label indicated the unbiased model, while the others the troposphere-biased model with different biases. The subplots from *left* to *right* denote the ionosphere-weighted CORS, static and kinematic baseline models with varying STDs of ionospheric constraints for the unbiased and troposphere-biased cases

Table 1 The maximum relative ZTD biases the troposphere-biased model can tolerate to obtain better AR performance than the unbiased model

σ_ι [cm]	Max. Bias τ [cm]			
	3.5	7.0	14	∞
CORS	1.0 (b)	1.0 (u)	1.0 (u)	0.5 (u)
Static	3.0 (b)	2.5 (b)	2.0 (–)	1.5 (u)
Kinematic	3.0 (b)	2.5 (b)	2.0 (–)	1.5 (u)

The recommended choice between troposphere-biased (b) and unbiased (u) model is indicated, where (–) means that there is no clear preference

depends on how representative the results from Fig. 6 are in a particular situation; especially for baselines with large height differences or in case of different atmospheric circumstances, it should first be assessed what realistic values are for the actual relative ZTDs.

For baselines shorter than 25 km, i.e., with $\sigma_\iota \leq 3.5$ cm, it is recommended to use the troposphere-biased model for all three baseline models. As shown in Fig. 6, the relative ZTDs will then be as small as a few millimeters, much smaller than the maximum allowed biases presented in Table 1. From this figure, it follows that up to a baseline length of 50 km, the relative ZTD will be below 1.5 cm,

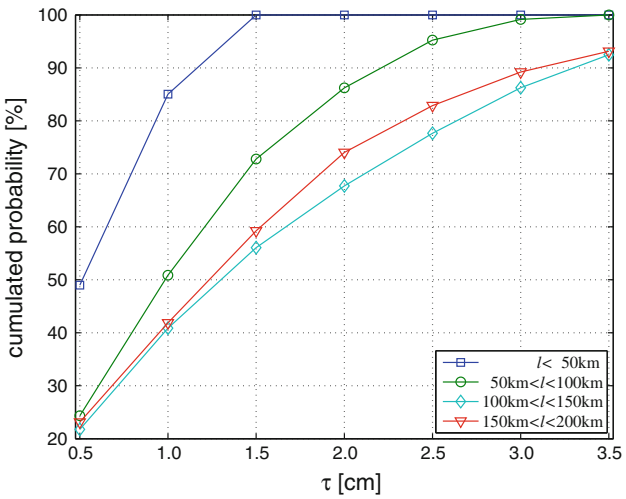

Fig. 6 The cumulative probability distribution of the relative ZTDs for different intervals of the baseline length (ℓ)

which is smaller than the maximum bias for the static and kinematic baseline models.

With a CORS model, more caution is needed; it is recommended to only use the biased model for short baselines, below 25 km, and for longer baselines to use the unbiased model.

According to Fig. 6, the relative ZTD for medium-length baselines between 50 and 100 km is generally below 2.5 cm. The corresponding maximum biases for $\sigma_\iota \leq 7.0$ cm in Table 1 are larger for the static and kinematic baseline models. Hence, again it is recommended to use the biased model.

For baselines longer than 100 km, the relative ZTDs will generally be larger than the maximum allowed biases in Table 1 ($\sigma_\iota = 14.0$ cm or ∞). It is then better to use the unbiased model for AR.

Ambiguity resolution with ionospheric biases

Similar to the study of troposphere-biased ambiguity resolution, we study the ambiguity resolution in the absence and presence of ionospheric biases in this section. We first present the unbiased and ionosphere-biased models. Then, the performance of ionosphere-biased model is numerically demonstrated by comparing with the unbiased model, and the maximum biases are also analyzed for difference cases.

Unbiased and ionosphere-biased model

The unbiased kinematic baseline model to be considered here is the same ionosphere-weighted model presented in section "Unbiased and troposphere-biased model," Eqs. (20) and (21). Equivalently, the unbiased CORS and static baseline models are identical. To present the ionosphere-biased model, we take an assumption that the ionospheric corrections, $\boldsymbol{\iota}_k^0$, are deterministic, i.e., $Q_{\boldsymbol{\iota}\boldsymbol{\iota}} = \mathbf{0}$. However, in the event that there is an error in the ionospheric corrections, $\Delta\boldsymbol{\iota}_k = \boldsymbol{\iota}_k - \mathrm{E}(\boldsymbol{\iota}_k^0) \neq 0$, this leads to the biased estimation. The corresponding biased kinematic baseline model reads

$$\mathrm{E}(\bar{\boldsymbol{y}}_k) = \boldsymbol{A}\boldsymbol{a} + \boldsymbol{B}_k\boldsymbol{b}_k + \boldsymbol{G}_k\tau, \quad \mathrm{D}(\bar{\boldsymbol{y}}_k) = \boldsymbol{Q}_{\boldsymbol{y}_k\boldsymbol{y}_k} \tag{22}$$

where $\bar{\boldsymbol{y}}_k = \boldsymbol{y}_k - \boldsymbol{E}\boldsymbol{\iota}_k^0$ is the observation vector with ionospheric corrections applied. The reason to work with $\bar{\boldsymbol{y}}_k$ is that the corrections are assumed deterministic, and consequently, no ionosphere parameters need to be estimated. In this way, the biased model still has the same structure as in (6).

The ionospheric delay $\boldsymbol{\iota}_k$ is expressed as a function of the SD zenith ionospheric delay $\iota_{k,z}$,

$$\boldsymbol{\iota}_k = \boldsymbol{D}^T\boldsymbol{M}_k\iota_{k,z} \tag{23}$$

where $\boldsymbol{D}^T$ is used to convert the SD ionosphere biases to the DD ones. The mapping matrix $\boldsymbol{M}_k$ is applied to map $\iota_{k,z}$ to the SD slant ionospheric delays of all satellites with the ith element as (Leick 2004)

$$M_k(i) = \left[1 - \frac{R_e^2\cos^2\theta_k(i)}{(R_e + h_I)^2}\right]^{-1/2} \tag{24}$$

where $R_e = 6{,}371$ km is the average radius of the earth. $h_I = 350$ km is the mean ionosphere height. The angle $\theta_k(i)$ is the mean elevation of the ith satellite for the two baseline receivers. Furthermore, in the following, it will be assumed that the zenith ionospheric delay is constant for r epochs, i.e., $\iota_z = \iota_{k,z}$, for $k = 1,\ldots,r$. Hence, in the unbiased model (20), we have that $\boldsymbol{\iota}_k = \boldsymbol{D}^T\boldsymbol{M}_k\iota_z$.

The same mapping (24) can be applied to the ionospheric biases as well:

$$\Delta\boldsymbol{\iota}_k = \boldsymbol{D}^T\boldsymbol{M}_k\Delta\iota_z$$

If $\Delta\iota_z = 0$ holds true indeed, one can then compute the unbiased solution by using the reduced model (22). However, if $\Delta\iota_z \neq 0$, the model (22) is referred to as the ionosphere-biased model, and of course, a biased solution will be computed. As compared to model (1), here the bias $\nabla = \Delta\iota_z$.

In this section, the ionosphere-biased AR performance is examined and compared with the unbiased ionosphere-weighted model. The parameters used for the simulations are the same as those in section "Ambiguity resolution with tropospheric biases." Besides the dual-frequency cases, the single-frequency cases are studied for short baseline since then the residual ionospheric biases can have a large impact.

Simulation results

Similar to the troposphere-biased study, the TTFFs are determined for unbiased and ionosphere-biased models with varying biases. Figure 7 shows the mean TTFFs for all cases.

The results reveal overall the very high model strength for the ionosphere-biased models, such that instantaneous AR is achievable with all dual-frequency models for the SD zenith ionospheric bias $\Delta\iota_z$ as large as 5 cm. This holds true for the single-frequency CORS model as well. Although the single-frequency static and kinematic models take longer TTFFs compared to the dual-frequency case, they can still outperform the unbiased model if the bias is smaller than 10 cm.

The TTFF statistics in Fig. 7 are similar for both static and kinematic models, which is attributed to their comparable model strength as explained for the troposphere-biased case. Note that the STD of ionospheric correction only applies to the unbiased ionosphere-weighted model but not to the ionosphere-biased model anymore. That is why the same result is obtained with the dual-frequency ionosphere-biased models for both $\sigma_\iota = 3.5$ and 7.0 cm.

From Fig. 7, it can be observed that the TTFF with ionosphere-biased AR is either very small or extremely

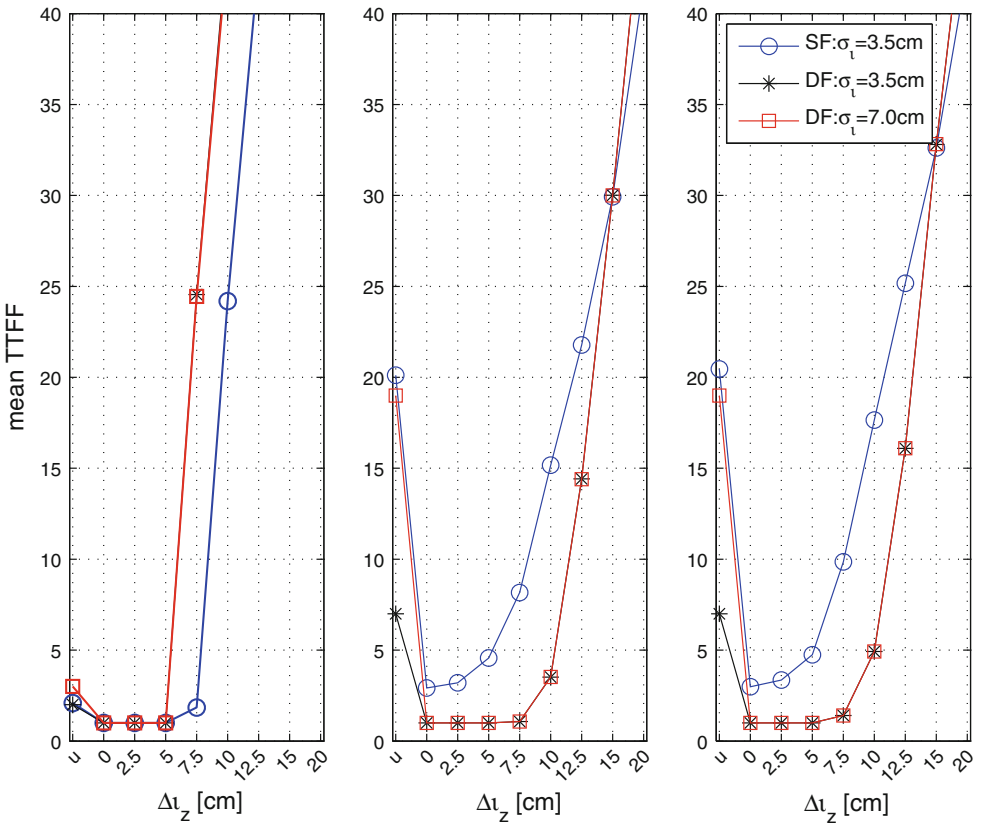

Fig. 7 The mean TTFFs as function of $\Delta\iota_z$. The "u" at *x*-label indicated the unbiased model, while the others the ionosphere-biased model with different biases. The subplots from *left* to *right* denote the CORS, static and kinematic baseline AR models with varying STDs of ionospheric constraints for unbiased and ionosphere-biased cases. DF and SF stand for dual- and single-frequency, respectively

large. The TTFF will become extremely large once a certain model-specific bias is exceeded. The reason is that the ionosphere-biased AR model is very strong, i.e., the corresponding PDF is very peaked. In this case, a small bias will hardly change the AR success rate as most of the probability mass will still be inside the correct pull-in region. However, when the bias exceeds a certain threshold, nearly all the probability mass will shift to the incorrect pull-in region, and consequently, the success rate will suddenly become very small. Further improving the model strength with more epochs will not help since the PDF already is very peaked. This behavior is illustrated in Fig. 2 with very small $\sigma_{\hat{a}}$, and the bias threshold in this one-dimensional case is 0.5 cycles.

It is now interesting to know how large the biases can be such that ionosphere-biased AR performance is still better than or at least comparable to the unbiased case. Therefore, for each of the 1,440 computation times, the SD zenith ionospheric bias $\Delta\iota_z$ is increased with steps of 0.2 mm up to a value of 40 cm until it is found that the TTFF exceeds the corresponding TTFF in the unbiased case. The histograms of the maximum allowable biases found in this way are shown in Fig. 8. The corresponding 95-percentile values of the maximum biases are presented in Table 2.

The maximum biases with the static and kinematic models are comparable, which is again attributed to their similar model strength. The maximum biases with the CORS model are relatively smaller due to the very high model strength for both the unbiased and biased models and thus the shorter TTFF; especially then the effect of transition from very short to extremely long TTFF is very sharp, see the left panel of Fig. 7.

The maximum biases with $\sigma_\iota = 7$ cm are larger than those with $\sigma_\iota = 3.5$ cm for all three models due to the shorter TTFFs with unbiased AR for $\sigma_\iota = 3.5$ cm compared to $\sigma_\iota = 7$ cm. Recall that with biased AR, no uncertainty in the ionospheric correction is assumed, and thus, the same performance applies. Of course, in reality, larger biases can be expected for longer baselines, see section "Choice of ionosphere-biased or unbiased model".

Compared with the dual-frequency case, the maximum bias with the single-frequency CORS model is larger, whereas those of single-frequency static and kinematic models are smaller, see Table 2. This result can be explained by the fact that the CORS model strength is mainly driven by the number of epochs and the number of frequencies. With the unbiased dual-frequency CORS model, the TTFF is very short, while for the single-frequency model, a few more epochs are required. This also means that, compared to the dual-frequency case, the TTFF can be larger in order to obtain better performance with the biased single-frequency model. And apparently, the

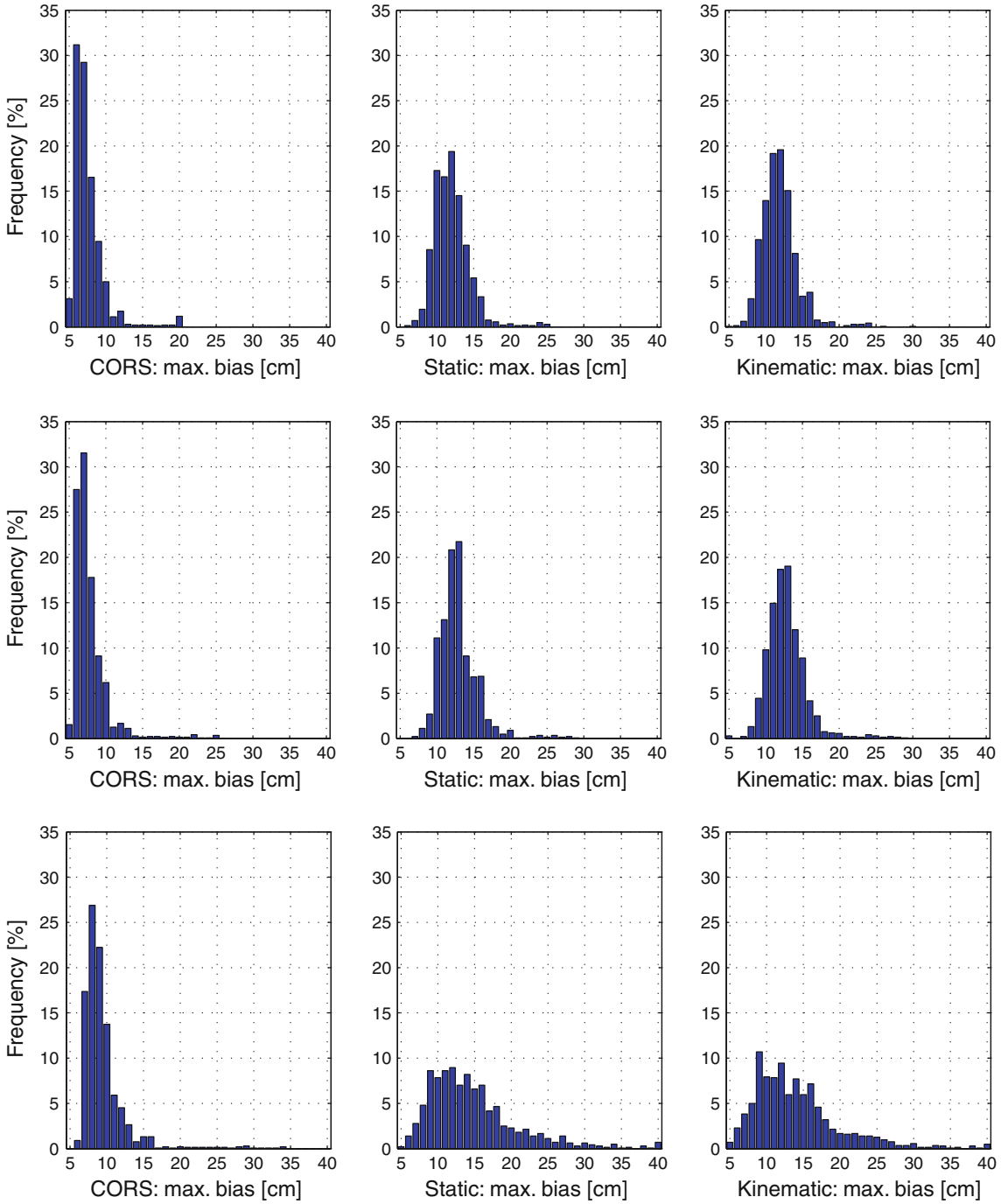

Fig. 8 The histogram of the maximum SD zenith ionospheric biases $\Delta\iota_z$ the ionosphere-biased model can tolerate to obtain better AR performance than with the unbiased model. The *top* and *middle row panels* are the dual-frequency results with $\sigma_\iota = 3.5$ cm and 7 cm in the unbiased model, respectively. The *bottom row panel* is the single-frequency result with $\sigma_\iota = 3.5$ cm. The *column panels* from *left* to *right* indicate the results with respect to the CORS, static and kinematic models, respectively

precision improvement due to the additional epochs generally has a larger impact than the bias (<6.7 cm) on the success rate. This effect does not apply to the static and kinematic models, where longer TTFFs are required, and the model strength is driven by the satellite-receiver geometry as well.

Choice of ionosphere-biased or unbiased model

Generally speaking, the ionospheric biases are proportional to the baseline length ℓ in real situations, and the following linear function is often used to describe the STD of ionospheric biases (Schaffrin and Bock 1988; Odijk 2002)

Table 2 The 95-percentile of maximum SD zenith ionospheric biases the ionosphere-biased model can tolerate to obtain better AR performance

	σ_ι [cm]	Max. Bias $\Delta\iota_z$ (cm)		
		CORS	Static	Kinematic
SF	3.5	6.7 (b)	7.4 (b)	6.4 (b)
DF	3.5	5.5 (b)	8.5 (b)	8.7 (b)
	7.0	5.6 (u)	9.6 (–)	9.2 (–)

The recommended choice between ionosphere-biased (b) or unbiased (u) model is indicated, where (–) means that there is no clear preference

$$\sigma_\iota = \beta\ell, \quad \text{with } 0.3 \text{ mm/km} \leq \beta \leq 3 \text{ mm/km} \tag{25}$$

The choice of β depends on the ionospheric activity as well as on the network data and processing; especially the impact of the ionospheric activity is difficult to capture due to its variability. A small value should be chosen during solar minimum periods, while large during solar maximum years. But it is still a troublesome task, because the ionospheric variation is rather complicated and even significantly differs from time to time during one day. Still, β can be empirically determined from the ionospheric delays estimated using real data. Odijk (2000) suggested $\beta = 0.57$ mm/km using the GPS data from a California network in the USA with 6 stations in quiet ionospheric conditions. Liu and Lachapelle (2002) made a similar but more extensive analysis using real data of 2 days from a 25-station Swedish GPS network. During these 2 days, there were times of low and high ionospheric activity, and the corresponding results were $\beta = 0.74$ and $\beta = 1.04$ mm/km, respectively.

With the latter values, the $2\sigma_\iota$ values, i.e., 95 % confidence levels, are between 3.7 and 5.2 cm for a baseline of 25 km. Hence, the value of $\sigma_\iota = 3.5$ cm used for the unbiased model in this study is conservative. Furthermore, it can be seen that these $2\sigma_\iota$ values are smaller than the maximum biases for the short baseline models in Table 2 (represented by $\sigma_\iota = 3.5$ cm). Therefore, it can be recommended to use the ionosphere-biased model for AR for short baselines in all cases.

For a baseline of 50 km, the $2\sigma_\iota$ values range from 7.4 to 10.4 cm. The maximum allowable bias with the CORS model is smaller, and thus, AR with the ionosphere-biased model should not be applied. For the static and kinematic baselines, biased AR may still be preferred under quiet ionospheric conditions, but in case of high ionospheric activity, the unbiased model must be used. It is noticed that for longer baselines, the ionospheric biases will be even larger and obviously reliable AR with the biased model is not feasible.

Finally, it should be emphasized that the choice of σ_ι for the unbiased model in real applications should reflect the actual uncertainty of the ionospheric corrections. A conservative value is advisable in order to account for the large fluctuations in ionospheric delays that can be present even over short times, and it should be avoided that the resulting SD ionospheric biases propagate in the ambiguity and baseline estimates.

Concluding remarks

The aim of this study has been to assess under which conditions the AR performance will be better when atmospheric biases are ignored. The enhanced model strength due to reduced number of unknown parameters is traded off against the impact of the bias on the AR success rate. Both the troposphere-biased and ionosphere-biased AR performance are studied quantitatively for CORS, static and kinematic baseline models with different settings and are compared to the corresponding unbiased ones. As a result, the maximum allowable bias is determined, such that the TTFF with the biased model is shorter than with the unbiased model. The TTFF is equal to the number of epochs required to obtain a success rate larger than 99.5 %.

The following recommendations can be made based on the results: (1) for short baselines, both the troposphere-biased and ionosphere-biased models can be used in all cases; (2) for medium-length baselines, neither troposphere-biased nor ionosphere-biased models can be used for CORS AR. For static and kinematic models, the troposphere-biased model can be used, and the ionosphere-biased model only when the ionosphere is not very active; (3) for long baselines, neither troposphere-biased nor ionosphere-biased models can be used in general. Only if the tropospheric biases are expected to be small, the troposphere-biased model can still be used for static and kinematic models.

Acknowledgments This work has been executed in the framework of the Positioning Program Project 1.01 "New carrier phase processing strategies for achieving precise and reliable multi-satellite, multi-frequency GNSS/RNSS positioning" in Australia of the Cooperative Research Centre for Spatial Information. PJG Teunissen is the recipient of an Australian Research Council (ARC) Federation Fellowship (project number FF0883188). This support is gratefully acknowledged.

References

Allison T (1991) Multi-observable processing techniques for precise relative positioning. In ION GPS-91, Albuquerque, NM, pp 715–726

Dach R, Hugentobler U, Fridez P, Meindl M (2007) Bernese GPS software version 5.0. Astronomical Institute, University of Bern

de Jonge PJ, Tiberius CCJM (1996) The LAMBDA method for integer ambiguity estimation: implementation aspects, LGR-series, No. 12. Technical report, Delft University of Technology

de Jonge PJ, Teunissen PJG, Jonkman N, Joosten P (2000) The distributional dependence of the range on triple frequency GPS ambiguity resolution. In ION-NTM 2000, Anaheim, CA, pp 605–612

Feng Y (2008) GNSS three carrier ambiguity resolution using ionosphere-reduced virtual signals. J Geodesy 82:847–862
Goad CC (1992) Robust techniques for determining GPS phase ambiguities. In 6th Geodesy Symposium on Satellite Positioning, Columbus, Ohio, pp 245–254
Hatch R (1982) The synergism of GPS code and carrier measurements. In 3rd Int Geod Sympon Satellite Doppler Positioning, 2:1213–1231, Las Vegas, New Mexico
Hatch R, Jung J, Enge P, Pervan B (2000) Civilian GPS: the benefits of three frequencies. GPS Solut 3(4):1–9
Henkel P, Günther C (2010) Partial integer decorrelation: optimum trade-off between variance reduction and bias amplification. J Geodesy 84:51–63
Joosten P, Irsigler M (2003). GNSS ambiguity resolution in the presence of multipath. In the European navigation conference GNSS 2002, Graz, Austria
Joosten P, Teunissen PJG (2001) On the error sensitivity of the GPS ambiguity success rate. In KIS 2001, pp 409–414, Banff, Canada
Kubo N, Yasuda A (2003) How multipath error influences on ambiguity resolution. In Proceedings of ION GNSS 2003, Portland
Leick A (2004) GPS satellite surveying, 3rd edn. Wiley, New York
Li B, Teunissen PJG (2011) High dimensional integer ambiguity resolution: a first comparison between LAMBDA and Bernese. J Navig 64(S1):S192–S210
Li B, Feng Y, Shen Y (2010a) Three carrier ambiguity resolution: distance-independent performance demonstrated using semi-generated triple frequency GPS signals. GPS Solut 14(2):177–184
Li B, Shen Y, Feng Y (2010b) Fast GNSS ambiguity resolution as an ill-posed problem. J Geodesy 84(11):683–698
Li B, Feng Y, Shen Y, Wang C (2010c) Geometry-specified troposphere decorrelation for subcentimeter real-time Kinematic solutions over long baselines. J Geophys Res, 115(B11):B11404. doi:10.1029/2010JB007549
Liu GC, Lachapelle G (2002) Ionosphere weighted GPS cycle ambiguity resolution. In ION National Technical Meeting, San Diego, CA, pp 1–5
Nardo A, Huisman L, Teunissen PJG (2011) GPS+GLONASS CORS processing: the Asian-Pacific APREF case. In IUGG 2011, Melbourne, Australia
Odijk D (2000) Weighting ionospheric corrections to improve fast GPS positioning over medium distances. In ION GPS 2000, Salt Lake City, UT, pp 1113–1123
Odijk D (2002) Fast precise GPS positioning in the presence of ionospheric delays. Ph.D. thesis, Publications on Geodesy, 52, Netherlands Geodetic Commission, Delft
Schaffrin B, Bock Y (1988) A unified scheme for processing GPS dual-band phase observations. Bull Geodesique 62:142–160
Teunissen PJG (1993) Least squares estimation of the integer GPS ambiguities. In Invited lecture, section IV theory and methodology, IAG General Meeting, Beijing
Teunissen PJG (1995) The least-squares ambiguity decorrelation adjustment: a method for fast GPS integer ambiguity estimation. J Geodesy 70:65–82
Teunissen PJG (1999) An optimality property of the integer least-squares estimator. J Geodesy 73(11):587–593
Teunissen PJG (2001) Integer estimation in the presence of biases. J Geodesy 75:399–407
Teunissen PJG, Joosten P, Tiberius CCJM (2000) Bias robustness of GPS ambiguity resolution. In ION GPS 2000, Salt Lake City, pp 104–112
Teunissen PJG, Joosten P, Tiberius CCTM (2002) A comparison of TCAR, CIR and LAMBDA GNSS ambiguity resolution. In ION GPS 2002, Portland, OR, pp 2799–2808
Verhagen S, Joosten P (2003) Algorithms for design computations for integrated GPS—Galileo. In the European navigation conference GNSS 2003, Graz, Austria
Verhagen S, Li B (2012) LAMBDA software package: Matlab implementation, version 3.0. Delft University of Technology and Curtin University, Perth, Australia
Verhagen S, Odijk D, Boon F, López-Almansa J (2007) Reliable multi-carrier ambiguity resolution in the presence of multipath. In ION GNSS 2007, pp 339–350, Forth Worth, TX
Verhagen S, Li B, Teunissen PJG (2013) Ps-LAMBDA: ambiguity success rate evaluation software for interferometric applications. Comput Geosci 54:361–376
Vollath U, Birnbach S, Landau H, Fraile-Ordoñez JM, Martín-Neira M (1998) Analysis of three-carrier ambiguity resolution (TCAR) technique for precise relative positioning in GNSS-2. In ION GPS-98, Nashville, TN, pp 417–426

Author Biographies

Bofeng Li obtained his Ph.D. from and now a professor at Tongji University, China. He carried out 3 years of postdoctoral research at GNSS Research Center, Curtin University, Australia. His research interests include ambiguity resolution and real-time precise positioning using multi-frequency, multi-GNSS signals. He has been chaired the IAG 4.5.4 workgroup since 2012.

Sandra Verhagen obtained her Ph.D. from and is now an assistant professor at Delft University of Technology. Her research focuses on ambiguity resolution and integrity monitoring for real-time kinematic GNSS applications.

Peter J. G. Teunissen is a Federation Fellow of the Australian Research Council (ARC), Professor of Geodesy and Navigation and Head of CUT's Global Navigation Satellite System (GNSS) Research Lab. His current research focuses on multi-GNSS and the modelling of next generation GNSS for high-precision relative navigation and attitude determination.